A novel persulfate-photo-bioelectrochemical hybrid system promoting the degradation of refractory micropollutants at neutral pH

Zou, Rusen; Tang, Kai; Hambly, Adam ; Chhetri, Ravi Kumar; Yang, Xiaoyong; Xu, Mingyi; Su, Yanyan; Andersen, Henrik Rasmus; Angelidaki, Irini; Zhang, Yifeng

Published in:
Journal of Hazardous Materials

Link to article, DOI:
10.1016/j.jhazmat.2021.125905

Publication date:
2021

Document Version
Publisher's PDF, also known as Version of record

Journal of Hazardous Materials 416 (2021) 125905

Contents lists available at ScienceDirect

Journal of Hazardous Materials

journal homepage: www.elsevier.com/locate/jhazmat

A novel persulfate-photo-bioelectrochemical hybrid system promoting the degradation of refractory micropollutants at neutral pH

Rusen Zou [a], Kai Tang [a], Adam C. Hambly [a], Ravi Kumar Chhetri [a], Xiaoyong Yang [a], Mingyi Xu [a], Yanyan Su [b], Henrik Rasmus Andersen [a], Irini Angelidaki [a], Yifeng Zhang [a,*]

[a] Department of Environmental Engineering, Technical University of Denmark, DK-2800 Lyngby, Denmark
[b] Carlsberg Research Laboratory, Bjerregaardsvej 5, 2500 Valby, Denmark

ARTICLE INFO

Editor: Dr. J He

Keywords:
Persulfate-enhanced photo-bioelectrochemical system
UV
Synergistic effects
Refractory micropollutants
Eco-toxicity

ABSTRACT

Bio-electro-Fenton is emerging as an alternative technology for the efficient and cost-effective removal of refractory micropollutants. Though promising, there are still several challenges that limit its wide application, including acidic operating conditions (pH at 2–3), the addition of supporting electrolytes (e.g., Na_2SO_4), and the issue of iron sludge generation. To address these challenges, a novel hybrid persulfate-photo-bioelectrochemical (PPBEC) system is proposed to remove model micropollutants (carbamazepine and clorfibric acid), from secondary effluent at low persulfate (PS) dosage and neutral pH. The effect of crucial operating parameters on the process was studied, including input voltage, cathodic aeration velocity, and PS dose. Under optimal conditions (0.6 V, 0.005 mL min^{-1} mL^{-1} and 1 mM), the PPBEC system achieved approx. 0.56–1.71 times greater micropollutant removal with 93% lower energy consumption when compared to the individual processes (UV/PS and PBEC). The improved performance was attributed to a faster production of sulfate radicals by UV irradiation, hydrogen peroxide activation and single-electron reduction, and hydroxyl radicals generated by UV irradiation. Furthermore, the transformation products of carbamazepine and clorfibric acid were identified and the probable pathways are proposed. Finally, the ecotoxicity of the PPBEC treated effluent was assessed by using *Vibrio Fischeri,* which exhibited a non-toxic effect.

1. Introduction

In recent years, high levels of residual pharmaceuticals have been detected in municipal sewage due to the increasing global consumption of pharmaceuticals. This in turn brings new challenges to traditional sewage treatment facilities. Current wastewater treatment discharge standards do not typically have threshold limits for these refractory pharmaceuticals, which has resulted in their widespread detection in surface water, groundwater, and even drinking water (Monteil et al., 2019). As a consequence, long-term exposure to these refractory pharmaceuticals has had measurable adverse impacts on various organisms and even humans (e.g., spread distribution of antibiotic-resistant genes) (Pazda et al., 2019).

Among existing treatment methods, AOPs have received widespread attention due to their ability to efficiently eliminate refractory pharmaceuticals in a reliable manner, via the generation of free radicals with strong oxidizing capabilities, such as hydroxyl radicals (•OH). Recently, bioelectrochemical process-based AOPs, in particular bio-electro-Fenton (BEF) process, have become a focal point of AOP research due to several advantages. Firstly, they inherit the advantage of the traditional electro-Fenton (EF) process that can efficiently treat high-concentration (mg L^{-1} and even to g L^{-1}) pharmaceutical-containing wastewater through in situ production of •OH (Eq. (1)). Secondly, they are highly controllable and require only mild operating conditions. Thirdly, the energy consumption of BEF systems is typically low (Ahmed et al., 2017; Monteil et al., 2019).

$$2H^+ + O_2 + 2e^- \rightarrow H_2O_2 \quad (1)$$

Despite being such a promising technology, there are still several challenges that need to be addressed for BEF processes. Firstly, the use of iron as a catalyst in the BEF process can lead to iron sludge problems (Nadais et al., 2018). Additionally, as both EF and BEF processes are optimized at pH 2–3, pH adjustments are thus needed, both before and after treatment, which inevitably increases their operating costs.

* Corresponding author.
E-mail addresses: yifz@env.dtu.dk, yifzmfc@gmail.com (Y. Zhang).

https://doi.org/10.1016/j.jhazmat.2021.125905
Received 26 February 2021; Received in revised form 12 April 2021; Accepted 13 April 2021
Available online 16 April 2021

Furthermore, the addition of supporting electrolytes (e.g. Na_2SO_4) has been required to increase the current flow and the treatment efficiency. This can also increase direct operating costs, as well as requiring further downstream treatment (e.g. reverse osmosis) before discharge, to reduce potential negative effects on receiving water bodies (Nadais et al., 2018). These bottlenecks have so far restricted the wide application of BEF technology. Furthermore, the variability in quantity and quality of natural organic matter (NOM) and inorganic ions within real water matrices may also adversely affect the treatment due to the non-selectivity of •OH radicals, and their subsequent scavenging effect.

In addition to •OH, sulfate radicals ($\bullet SO_4^-$) have also been adopted in AOPs to oxidize organics due to their advantages of having longer reaction lifetimes, selective electron transfer, and ability to work efficiently over a wider pH range (2−8) (Pan et al., 2019; Xu et al., 2017). $\bullet SO_4^-$ can be generated by activating persulfate (PS) or permonosulfate (PMS) in a variety of ways, including the use of H_2O_2, transition metals, ultraviolet (UV) irradiation, visible light, etc (Wang and Wang, 2018a). Among them, UV irradiation has been shown as one of the most effective ways to activate PS or PMS. So far, the UV/PS process (Eq. (2)) has proven to be both more efficient and economical for the removal of refractory pharmaceuticals, than the UV/PMS process (Deng et al., 2013).

$$S_2O_8^{2-} \xrightarrow{hv} 2 \bullet S \tag{2}$$

However, the performance of the UV/PS process in the treatment of real wastewater is often limited because the wastewater characteristics including turbidity, chromaticity, and suspended solids could reduce the UV transmittance, thereby reducing the formation of $\bullet SO_4^-$. Besides, the removal efficiency of the UV/PS process is mainly dependent on the PS dosage. This increases both the treatment cost, as well as increases the production of SO_4^{2-} waste which requires further processing. In this context, the combination of the UV/PS process and the BEF process could not only greatly improve the removal efficiency but also overcome the shortcomings of the individual UV/PS process and the BEF process mentioned above. Specifically, photocatalysis by UV irradiation to eliminate pharmaceuticals can also be achieved through direct photolysis, or by activation of the cathodic H_2O_2 generated in situ, to produce •OH (Eq. (3)). These processes can also help to overcome the above-mentioned drawbacks in the BEF system, including the requirement for pH adjustment and iron sludge generation. Moreover, the activation of PS by the bioelectrochemical system could be enhanced to overcome the influence of UV transmittance (Durán et al., 2017), as it could also generate $\bullet SO_4^-$ by single-electron reduction reaction (Eq. (4)) and the cathodic in situ generated H_2O_2 activation (Eq. (5)). Furthermore, in some cases, the SO_4^{2-} waste can be further utilized as a cathodic supporting electrolyte for the bioelectrochemical system to increase the circuit current, and in turn, to enhance H_2O_2 production.

$$H_2O_2 \xrightarrow{hv} 2 \bullet OH \tag{3}$$

$$e^- + S_2O_8^{2-} \rightarrow \bullet SO_4^- + SO_4^{2-} \tag{4}$$

$$H_2O_2 + S_2O_8^{2-} \rightarrow \bullet SO_4^- + \bullet HO_2 + HSO_4^- \tag{5}$$

Herein, a novel hybrid PS enhanced photo bioelectrochemical (PPBEC) system was developed, by combining a bioelectrochemical system and a UV/PS process, to be used as a tertiary treatment process for the removal of refractory pharmaceuticals from the real WWTPs secondary effluent at neutral pH. This hybrid system could significantly improve the treatment performance, as well as save costs, over previously developed UV/PS and BEF processes.

Carbamazepine (CBZ) and clofibric acid (CA) have been widely detected in the various water types such as surface water and WWTPs effluent (ranging from ng·L^{-1} to μg·L^{-1}) around the world over recent decades (Calisto et al., 2011; Li et al., 2010). For example, it is reported that the highest CBZ concentration detected in surface water and groundwater were 11,561 and 390 ng L^{-1}, respectively (Moztahida et al., 2019). In addition, the content of CA detected in Canadian surface water ranges from 0.101 to 0.175 μgL^{-1} (Rebelo et al., 2020). It can be expected that these pollutants will continue to accumulate in the environment to higher concentrations in the long term due to missing of efficient treatment. In addition, by 2016 at least 631 pharmaceutical active compounds have been detected in various water bodies (Ramírez-Morales et al., 2020). The total concentration of these compounds can easily end up to several mg L^{-1}. In this study, a higher initial concentration (mg L^{-1} level) of CBZ and CA were selected as the model compounds for refractory pollutants to examine the treatment performance of the novel PPBEC system. Furthermore, these concentration gradients were selected in order to compare the results with the existing studies. In many recent studies on the removal of CBZ, the adopted concentrations are about 5–15 mg L^{-1} (Lai et al., 2021; Thanekar et al., 2018; Yang et al., 2021; Yu et al., 2021). The impact of operating parameters including input voltage, cathodic aeration velocity, and PS dosage on the removal of the CBZ and CA were then evaluated. The major transformation products were also investigated and the effluent ecotoxicity was assessed. Furthermore, the applicability of the PPBEC system for the removal of two model pharmaceuticals in different water matrices was also explored. Finally, the PPBEC system was compared to the UV/PS process, the BEF process, and other AOPs such as the EF process, from the perspective of both removal efficiencies and economic cost.

2. Experimental

2.1. Chemicals

For detailed information on the main chemicals used in this study, see Text S1 (supporting information). As for the detailed water characteristics of the 4 different water bodies, see Table S1.

2.2. PPBEC system setup and operation

A laboratory-scale PPBEC reactor was constructed, consisting of two identically-sized chambers where the effective size of each chamber was 8 cm × 5 cm × 5 cm (Fig. S1). Accordingly, the total volume of each chamber was 200 mL, with a working volume of 180 mL. The PPBEC design and materials for individual reactor components including the anode electrode (carbon brush), cation exchange membrane, and Ag/AgCl reference electrode in the cathode chamber, and the corresponding pretreatment methods were identical to those documented within our previous study (Nadais et al., 2018). In addition to these components, a commercial-grade graphite plate (4 cm × 4 cm) coated with carbon black was used as a gas diffusion cathode (GDC), and the specific preparation method was carried out as previously described (Yu et al., 2015). A detailed description of running the PPBEC system was shown in Text S2.

2.3. Analytical methods and calculations

The detection method for the in situ produced H_2O_2 was the same as has been previously described (Nadais et al., 2018). The CBZ and CA concentrations and the corresponding transformation products during the PPBEC system were quantified by high-performance liquid chromatography (Agilent 1290 Infinity, USA, HPLC) system coupled with a tandem mass spectrometer (Agilent 6470 series, USA, MS/MS). Detailed HPLC-MS/MS parameter settings were listed in Text S3. pH was monitored by a pH meter (PHM210, Radiometer, Denmark). The voltage across the 10-ohm resistor and the cathode potential was detected by a digital multimeter (Model 2700, Keithley Instruments, Inc., Cleveland, OH, USA), and the corresponding system current can be calculated by Ohm's law.

The removal of four selected model pharmaceuticals was followed by pseudo-first-order kinetics during the BEF process and UV/PS process

(Nadais et al., 2018), where the apparent rate constant (K_{app}) can be calculated via Eq. (6).

$$K_{app}t = \ln \frac{C_0}{C_t} \quad (6)$$

The electrical energy per order (E_{EO}) was adopted to express electric energy consumption, as it was most conducive for comparison with other AOPs in terms of energy consumption. The calculations of E_{EO} (see Text S4) were conducted as previously described (Pan et al., 2019). Specifically, the bulk of the treatment cost of the PPBEC process originated from two aspects, including electrical energy consumption; and (2) chemical reagent (PS) cost. To further facilitate comparisons, the energy consumption in this paper was divided into four parts including UV lamp consumption, MEC reactor consumption (direct voltage input), aeration, and agitation consumption on the treatment of WWTPs secondary effluent (Lyngby) spiked with CBZ and CA (10 mg L^{-1} of each). Calculations were based on the local electricity price (Denmark) and the PS price (0.25 € kWh^{-1} and 0.62 € kg^{-1}, respectively) and the corresponding total expenditure was further calculated in terms of cost per order ($Cost/O_{total}$).

Finally, one-way analysis of variance (one-way ANOVA) was carried out via SPSS 24.0 Statistics software (IBM Crop, USA) to analyze the significant difference among the obtained results. When the p value was < 0.05, the data were considered statistically significant.

2.4. Eco-toxicity assays

Microtox tests were conducted through a bioluminescence inhibition experiment, using *Vibrio fischeri* as the toxicity indicator (Zou et al., 2020b). This method was used to assess the ecotoxicity of both the secondary biological treatment effluent and the effluent from the novel PPBEC system.

3. Results and discussion

3.1. Synergistic effect of PBEC with UV/PS

Experiments were first conducted by comparing the degradation of CBZ and CA via several treatment processes including: a) UV irradiation only; b) PS addition only; c) microbial electrolysis cell (MEC); d) UV/PS; e) PBEC; f) PBEC with 50 mM Na_2SO_4 addition; and g) PPBEC (Fig. 1). As shown in Fig. 1, the reactor itself and the electrodes have a negligible adsorption effect on CBZ and CA. It was found that removal of both CBZ (about 4% and 6% in 8 h, respectively) and CA (about 2% and 3% in 8 h, respectively) were very low by only PS addition and MEC processes. This is due to the weak oxidation ability of H_2O_2 synthesized within the MEC process and directly added PS. This finding is consistent with previous studies regarding the removal of emerging pharmaceuticals during UV/PS and BEF processes (Bu et al., 2016; Zou et al., 2020a). Furthermore, it was found that CBZ was still not easily removed by direct UV irradiation alone (7% after 8 h). In contrast, CA was better degraded by these methods (65% after 8 h), which was also consistent with previous literature (Ali et al., 2018; Lu et al., 2018). As depicted in Eq. (7) and Eq. (8), the degradation of CBZ and CA under direct UV irradiation can be divided into two steps. Firstly, the aromatic rings and heteroatoms such as nitrogen and chlorine are promoted to an electronically excited state under UV irradiation (254 nm) (Eq. (7)), which then react to form a new product through chemical decomposition (Ali et al., 2018; Carlson et al., 2015; Khan et al., 2017) (Eq. (8)). Unlike CA, CBZ contains an amide group ($RCONH_2$), which makes further degradation difficult (Ali et al., 2018). The observed degradation of CA under direct UV photolysis was consistent with previous reports, and is in line with pseudo-first-order kinetics with a rate constant (K_{app}) of 0.128 h^{-1} (R^2 =0.97) (Khan et al., 2014).

$$CBZ\ (CA) \xrightarrow{hv} CBZ*\ (CA*) \quad (7)$$

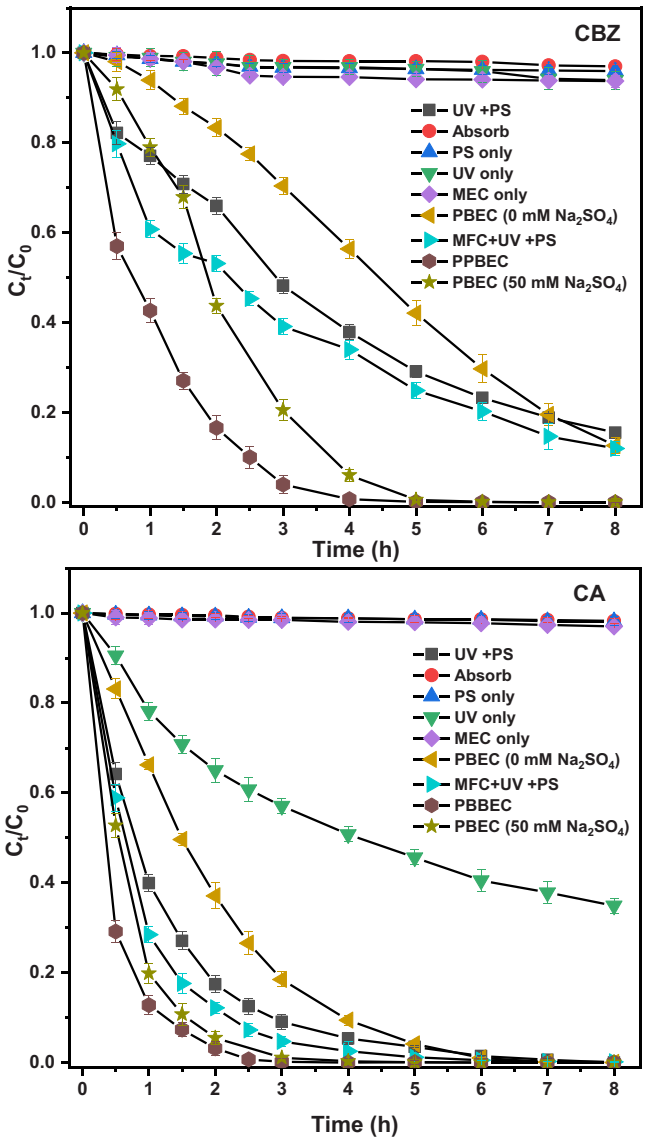

Fig. 1. Comparison of the removal of CBZ and CA through different treatment methods. System operational parameters: The initial CBZ and CA concentrations of 10 mg L^{-1} were spiked into the WWTPs secondary effluent (Lyngby), and other parameters were determined based on the earlier described tests, including PS dosage of 1 mM, applied voltage of 0.6 V, cathodic aeration velocity of 0.005 mL min mL^{-1}, UV intensity of 10 mW cm^{-2} and without pH adjustment.

$$CBZ* \ (CA*) \rightarrow by-products \quad (8)$$

Since individual PS oxidation or MEC processes could not effectively remove CBZ and CA, and direct UV photolysis was also ineffective towards CBZ, further processes including PBEC (both with and without 50 mM Na_2SO_4 addition), UV/PS, and PPBEC were also investigated. In the UV/PS process, degradation was significantly enhanced, achieving approximately 84.5% and 100% within 8 h for CBZ and CA, respectively. This can be attributed to the fact that the bond of O-O in PS is broken under UV irradiation due to the production of $\bullet SO_4^-$ containing a lone pair of electrons via Eq. (2). This then has a strong oxidation ability, and can therefore quickly degrade both CBZ and CA (Gao et al., 2012). The PBEC process also showed a clear improvement in CBZ and CA removal, both with and without the addition of 50 mM Na_2SO_4. Here, the pharmaceuticals removal efficiency during the first 8 hrs without 50 mM Na_2SO_4 addition was approximately 87.5% and 100% for CBZ

and CA, respectively. The efficiency was increased to 100% for both compounds within 5 h, with the addition of 50 mM Na_2SO_4 to the process. Similarly, as the UV/PS process was described above, PBEC can effectively remove CBZ and CA due to the in situ generation of H_2O_2. Under UV irradiation via Eq. (2), H_2O_2 is converted to •OH, which has an even stronger oxidation ability than $•SO_4^-$ (Yuan et al., 2009). The addition of Na_2SO_4, resulted in the improvement of cathodic conductivity (from 1.45 to 7.81 ms cm^{-1}) and subsequently led to the increase of system current (from approximately 2.25 to 5.50 mA, Fig. S2). This ultimately resulted in an increased yield of H_2O_2 and •OH for the degradation of CBZ and CA (Li et al., 2018; Moreira et al., 2017).

The degradation of CBZ and CA during the above processes were found to follow pseudo-first-order kinetics. The K_{app} values of CBZ were 0.235 (R^2 =0.99), 0.255 (R^2 =0.97) and 0.699 (R^2 =0.93) h^{-1}, followed by the K_{app} values of CA were 0.683 (R^2 =0.99), 0.731 (R^2 =0.97) and 1.476 (R^2 =0.99) h^{-1} where each value corresponds to UV/PS, PBEC and PBEC (with 50 mM Na_2SO_4) processes, respectively. Although the PBEC process with the addition of 50 mM Na_2SO_4 achieved the highest removal efficiencies for our target pollutants, in practice the addition of such a high concentration of salts would require further processing before discharge, and hence limit its wide application.

Fortunately, this limitation could be overcome by the addition of PS in place of Na_2SO_4. PS can be activated to produce $•SO_4^-$ for the pollutants removal, as well as SO_4^{2-} (as a reaction product) that can increase water conductivity, and thus, promote H_2O_2 generation. As such, the synergistic effect of $•SO_4^-$ and •OH can be maintained along with the subsequently improved removal efficiencies. Durán et al. found that the UV/H_2O_2/PS process can increase pollutant removal rates by more than 10% compared to the UV/H_2O_2 process (Durán et al., 2017). Additionally, Pan et al. found that the pollutants removal efficiency in UV/pre-Fe^0/PS process was over 2.2 times higher than that of the UV/Fe^0/PS process. In both cases, the improvement of removal was mainly attributed to the production of more $•SO_4^-$ and •OH (Pan et al., 2019). Interestingly, our PPBEC process showed significantly higher removal rates of CBZ and CA than those reported in the aforementioned studies ($p < 0.05$). In the PPBEC system, the K_{app} values increased to 1.326 (R^2 =0.99) and 2.199 (R^2 =0.98) h^{-1} for CBZ and CA, respectively. This is a significant improvement of system performance (over UV/PS or PBEC processes) and can be attributed to the synergistic effect of $•SO_4^-$ and •OH. This was confirmed by the high synergy factor values (1.706 for CBZ and 0.555 for CA), that were calculated based on previous literature (Pan et al., 2019). A stable system current output (Fig. S2) demonstrated the stability of the bioanode-based PBEC system, as well as for the derived PPBEC system. Due to the use of bipolar membranes, the pH of the entire treatment process increased slightly (from 7.60 to 8.28, Fig. S2). Unlike the traditional EF and BEF processes, pH adjustment was therefore not required. Overall, the PPBEC process was proven the most effective method for the removal of selected pollutants.

3.2. Impact of operating parameters on the removal of CBZ and CA

3.2.1. Applied voltage

The circuit current is directly related to the rate of H_2O_2 generation from the cathode (Eq. (1)), which can subsequently affect the formation of •OH (Xu et al., 2016; Zhao et al., 2017). Therefore, The PPBEC process was further investigated at a range of applied voltages (0, 0.2, 0.4, 0.6, and 0.8 V). As shown in Fig. 2, the removal of CBZ and CA by the PPBEC process was significantly affected by different applied voltages ($p < 0.05$, Table S3). Specifically, the removal rate of CBZ and CA was positively correlated with the applied voltage in the range of 0–0.6 V (current increased from 0.68 to 4.40 mA, Fig. S3), which is likely due to the increase of H_2O_2 production as noted above. The enhanced H_2O_2 production in turn lead to more •OH formation under UV irradiation. Moreover, it may also lead more $•SO_4$ production because H_2O_2 can also react with PS to produce further radicals including $•SO_4^-$ and $•HO_2$ via

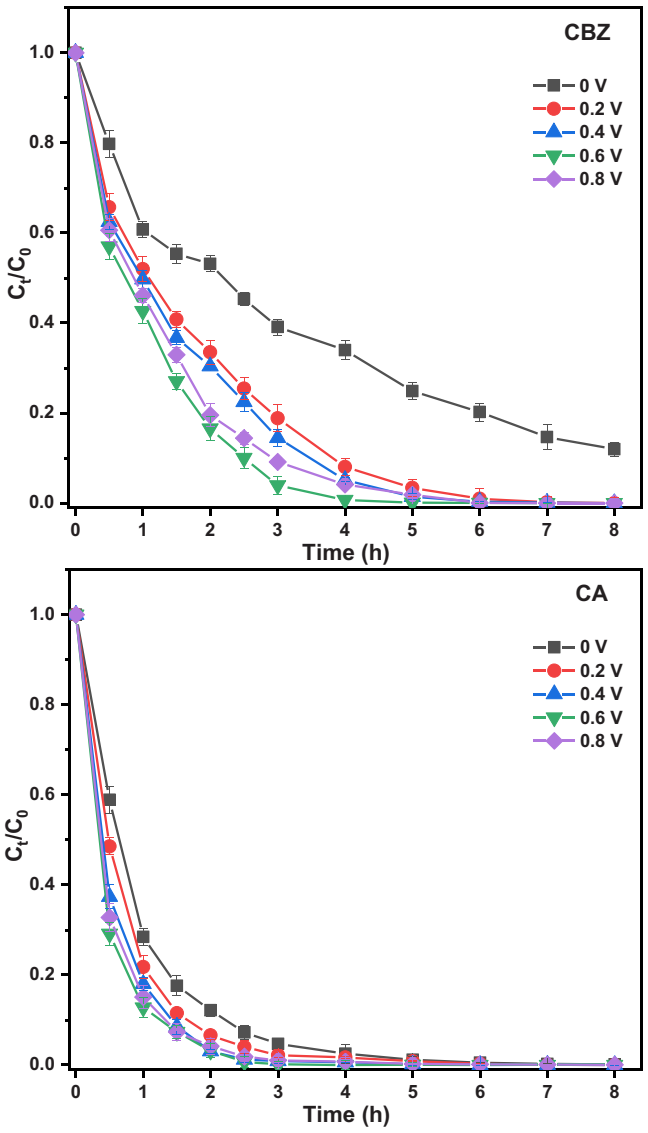

Fig. 2. The impact of applied voltage on system performance. System operational parameters:.
The initial CBZ and CA concentrations of 10 mg L^{-1} were spiked into the WWTPs secondary effluent (Lyngby), and other parameters were determined based on the earlier described tests, including PS dosage of 1 mM, cathodic aeration velocity of 0.005 mL min mL^{-1}, UV intensity of 10 mW cm^{-2} and without pH adjustment.

Eq. (5), thereby improving the removal efficiency of CBZ and CA (Durán et al., 2017).

However, when the voltage was further increased from 0.6 to 0.8 V (corresponding to 5.05 mA, Fig. S3), the removal efficiency of CBZ and CA showed a downward trend. The K_{app} values followed the same trend, where the removal of CBZ and CA first reached to the maximum value at 0.6 V (1.326, R^2 =0.99) and (2.199, R^2 =0.98)), and then started to decline at 0.8 V. There are a number of factors which could contribute to the decreasing of removal efficient at high voltage. Firstly, if the current was too high, it may trigger side reactions including Eqs.(9–11) and reduce the production of H_2O_2 and further the formation of •OH and $•SO_4^-$ (Chen et al., 2015; Moreira et al., 2017; Oturan et al., 2018; Zou et al., 2021).

$$2\,H^+ + 2e^- \rightarrow H_2 \quad (9)$$

$$H_2O_2 + 2\,H^+ + 2e^- \rightarrow 2\,H_2O \quad (10)$$

$$2\ H_2O_2 \rightarrow 2\ H_2O + O_2 \quad (11)$$

Secondly, excess of H_2O_2 may further react with radicals including •OH and $•SO_4^-$ via Eqs. (12–16), thereby resulting in an effective decrease of H_2O_2, •OH and $•SO_4^-$ (Durán et al., 2017; Lin et al., 2016).

$$H_2O_2 + •OH \rightarrow •HO_2 + H_2O \quad (12)$$

$$H_2O_2 + •OH \rightarrow •O_2^- + H^+ + H_2O \quad (13)$$

$$•HO_2 + •OH \rightarrow O_2 + H_2O \quad (14)$$

$$H_2O_2 + •SO_4^- \rightarrow •HO_2 + SO_4^{2-} + H^+ \quad (15)$$

$$•HO_2 + •SO_4^- \rightarrow O_2 + SO_4^{2-} + H^+ \quad (16)$$

The residual H_2O_2 concentrations observed under different input voltages could further support the above explanation (Fig. S3) could support this explanation. From the above results, 0.6 V was considered as the most appropriate input voltage for the PPBEC process.

3.2.2. Cathodic aeration velocity

As illustrated in Eq. (1), cathodic O_2 supply can be another crucial operational parameter affecting the synthesis of H_2O_2 and the pharmeceuticals removal. Therefore, the impact of O_2 supply on the performance of the PPBEC process was further studied at varied cathodic aeration velocities ranging from 0 to 4 mL min^{-1} (corresponding to 0–0.02 mL min^{-1} mL^{-1}). As shown in Fig. 3, the removal efficiency of CBZ and CA was initially improved when the aeration velocity was raised from 0 to 0.005 mL min^{-1} mL^{-1}, and then subsequently dropped when the aeration velocity was further increased to 0.01 and even 0.02 mL min^{-1} mL^{-1}. One-way ANOVA ($p < 0.05$, Table S3) further showed a statistically significant difference in aeration rates between the four selected groups, suggesting that the contribution of O_2 was significant. This pattern was likely due to the introduction of proper cathodic aeration, which may maintain the dissolved O_2 concentration in the catholyte, and thus maintain the synthesis of H_2O_2 for better removal efficiency than that without aeration. However, when the aeration velocity was further increased, the amount of bubbles also increased, and this, in turn could increase the internal resistance of the system. The current decreased when the aeration velocity was increased to 0.01 and further to 0.02 mL min^{-1} mL^{-1} (Fig. S4), which is further evidence for this hypothesis (Luo et al., 2015; Zhou et al., 2013). Furthermore, the bubble sizes generated at faster aeration velocities were larger, which may hinder binding to the active site of the cathode(Liu et al., 2007). A faster aeration velocity may also lead to a decrease in UV radiation, which in turn reduces the production of $•SO_4^-$ and •OH for pharmaceuticals removal (Moreira et al., 2017). As a result of the above investigations, an aeration velocity of 0.005 mL min^{-1} mL^{-1} was deemed most appropriate and was therefore chosen for subsequent experiments.

3.2.3. PS dose in the cathode

Previous sections have discussed the impact of operating parameters related to the in situ production of H_2O_2 in the PPBEC process. The dosage of PS will clearly affect the generation of $•SO_4^-$, and thus, affect the overall treatment process. As such, the PPBEC system was further investigated with PS concentrations between 0 and 1 mM, as these concentration levels are commonly used in the individual PS process (Lu et al., 2018; Zhang et al., 2015). The removal efficiency of CBZ and CA during the PPBEC process increased as expected with the increase of PS dose from 0 to 0.75 mM (Fig. 4), whereafter only a slight improvement was achieved at 1 mM. Similar to the above, statistical analysis showed that it had a significant effect on CBZ and CA removal rates within the PS range studied ($p < 0.05$, Table S3). The whole process fitted well to pseudo-first-order kinetics. At concentrations of 0, 0.25, 0.5, 0.75 and 1 mM, the corresponding K_{app} values of CBZ were 0.255 (R^2 =0.99), 1.097 (R^2 = 0.94) 1.123 (R^2 = 0.99) 1.322 (R^2 = 0.93) and 1.326 (R^2 = 0.98) h^{-1}, while K_{app} values of CA were 0.731 (R^2 = 0.97), 1.590 (R^2 = 0.94) 1.694 (R^2 = 0.99) 1.958 (R^2 = 0.98) and 2.199 (R^2 = 0.98) h^{-1}. The overall improvement of CBZ and CA removal was mainly attributed to the production of more $•SO_4^-$ and •OH with the increase of PS dosage via Eqs. (2), (5) and (17) (Durán et al., 2017; Pan et al., 2019).

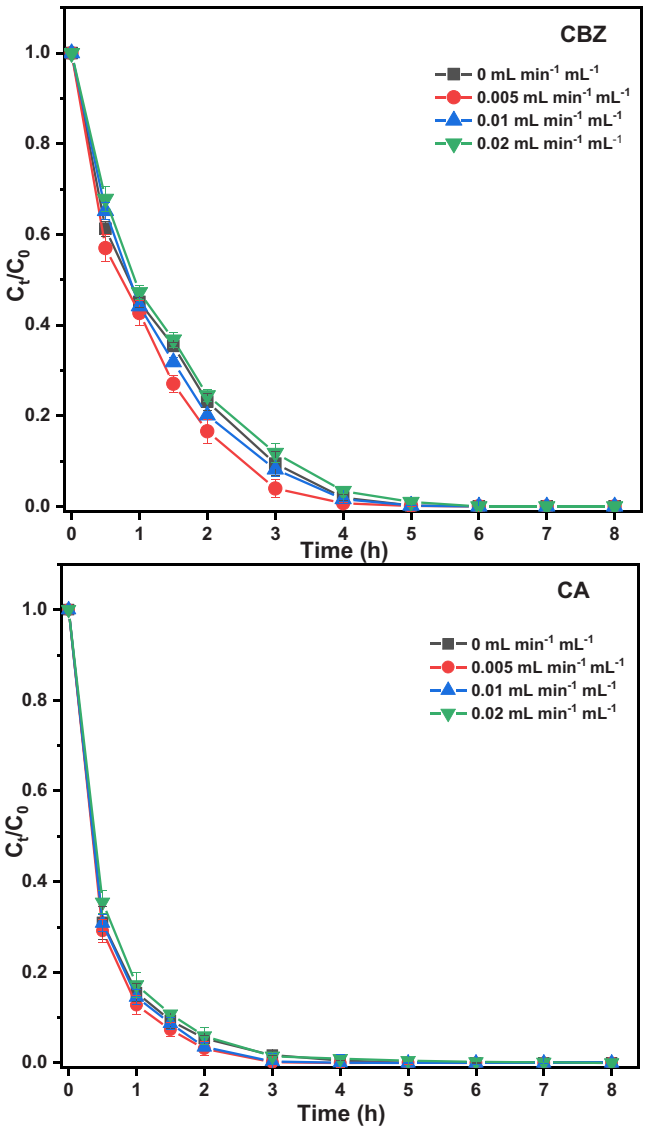

Fig. 3. The impact of cathodic aeration velocity on system performance. System operational parameters: the initial CBZ and CA concentrations of 10 mg L^{-1} were spiked into the WWTPs secondary effluent (Lyngby), and other parameters were determined based on the earlier described tests, including PS dosage of 1 mM, applied voltage of 0.6 V, UV intensity of 10 mW cm^{-2} and without pH adjustment.

$$•SO_4^- + H_2O \rightarrow SO_4^{2-} + •S_2O_8^{2-} \quad (17)$$

Along with the increase of PS dose, the conductivity of the catholyte and the system current both increased (Fig. S5), which resulted in more H_2O_2 production for •OH formation via Eq. (2). When further increasing the dosage of PS from 0.75 to 1 mM, the excessive PS might further consume the generated $•SO_4^-$ and •OH via Eqs. (18–20), thus the generated reactive radicals were not linearly related to the PS dosage within this higher range (Lu et al., 2018; Pan et al., 2019).

$$•SO_4^- + S_2O_8^{2-} \rightarrow SO_4^{2-} + •S_2O_8^{2-} \quad (18)$$

$$S_2O_8^{2-} + •OH \rightarrow •S_2O_8^{2-} + OH^- \quad (19)$$

$$•SO_4^- + •SO_4^- \rightarrow S_2O_8^{2-} \quad (20)$$

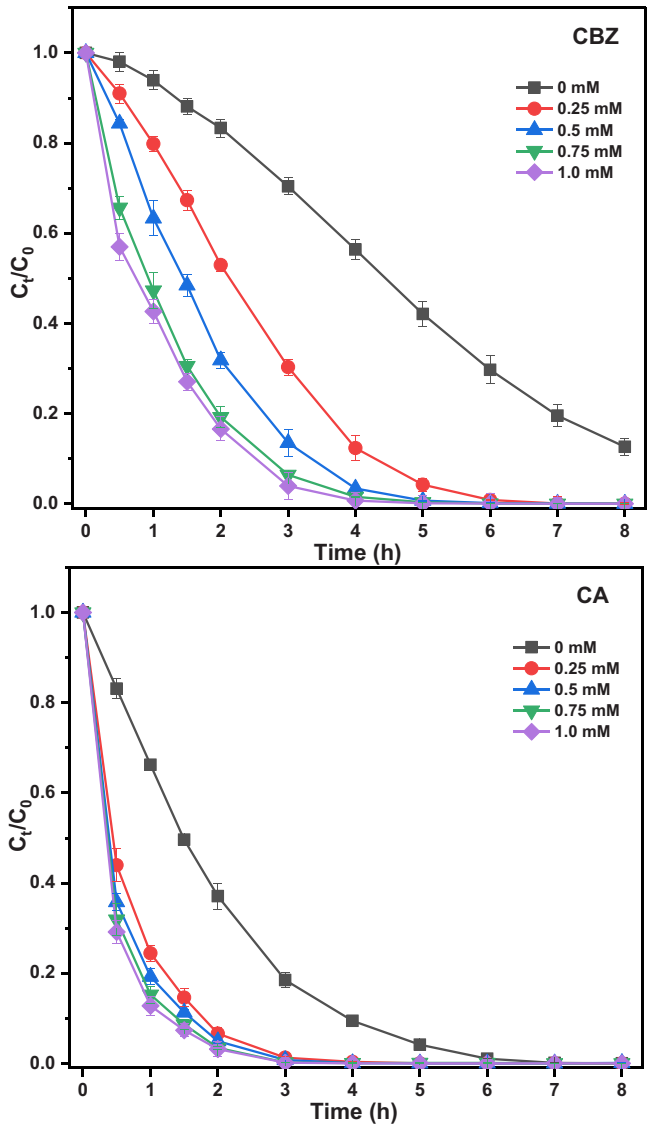

Fig. 4. The impact of PS dosage on system performance. System operational parameters: the initial CBZ and CA concentrations of 10 mg L^{-1} were spiked into the WWTPs secondary effluent (Lyngby), and other parameters were determined based on the earlier described tests, including applied voltage of 0.6 V, cathodic aeration velocity of 0.005 mL min mL^{-1}, UV intensity of 10 mW cm^{-2} and without pH adjustment.

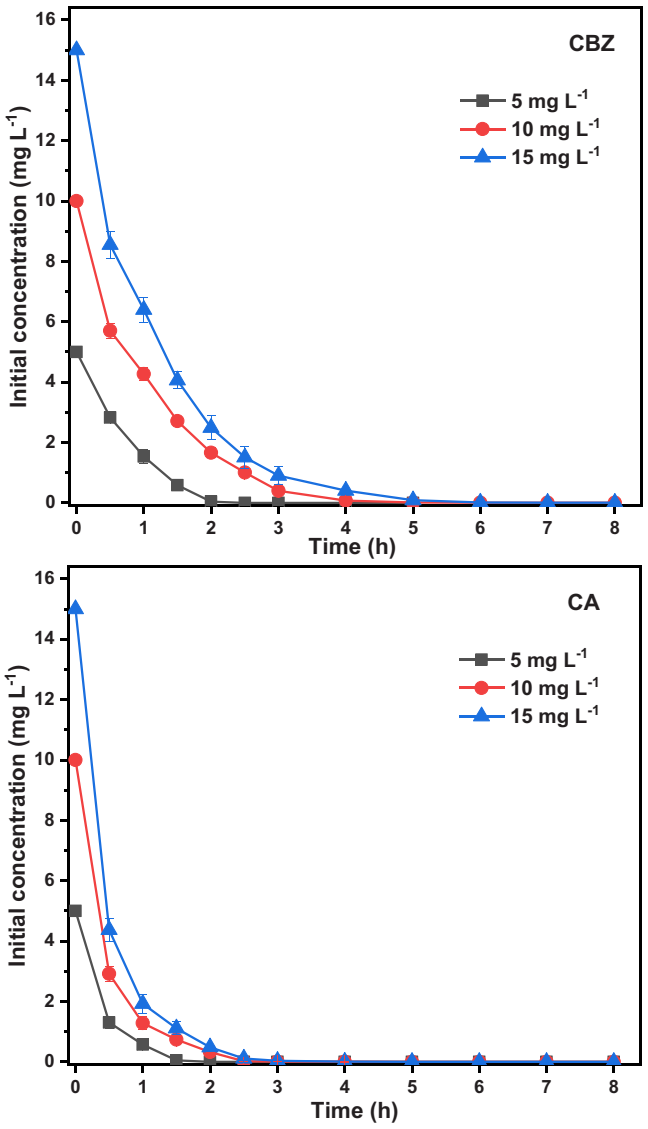

Fig. 5. The impact of initial CBZ and CA concentrations on system performance. System operational parameters: PS dosage of 1 mM, applied voltage of 0.6 V, cathodic aeration velocity of 0.005 mL min mL^{-1}, UV intensity of 10 mW cm^{-2} and without pH adjustment.

Taking into account that further increasing the PS dosage will not only enhance the above-mentioned suppression effect but also further increase the cost of chemicals, 1 mM was chosen as the optimal dose for the system.

3.2.4. *Initial CBZ and CA concentration*

Since the initial concentration of pollutants is regarded as one of the main influencing factors that determine the treatment capacity of AOPs, three concentration gradients of CBZ and CA (5, 10 and 15 mg L^{-1}) were selected to further evaluate the PPBEC process (Ali et al., 2018). Our results show that both CBZ and CA were completely removed within 6 h by the PPBEC process, within the selected concentration range (Fig. 5). The K_{app} values of CBZ were 1.401($R^2 = 0.98$), 1.326 ($R^2 = 0.98$) and 1.227 ($R^2 = 0.98$) h^{-1}, and the K_{app} values of CA were 2.958 ($R^2 = 0.96$), 2.199 ($R^2 = 0.98$) and 1.828 ($R^2 = 0.98$) h^{-1}, under initial concentration of 5, 10 and 15 mg L^{-1}, respectively. Then, one-way ANOVA further indicated that the studied initial concentration range had a significant impact on the removal rate of the selected pollutants ($p < 0.05$, Table S3). The observed trend in the calculated K_{app} values was also in agreement with previous studies on electrochemical or UV-based AOPs for the degradation of pollutants (Deng et al., 2013; Moreira et al., 2017). On one hand, higher initial concentrations mean that more intermediates could be produced under the same conditions. These, in turn compete with the parent compounds of CBZ and CA for the non-selective free radicals, mainly $\bullet SO_4^-$ and •OH, and thus may result in the reduction of the removal efficiency of the CBZ and CA (Chen et al., 2019; Deng et al., 2013). On the other hand, it may be that at higher initial concentrations, the concentration of CBZ and CA and their intermediates in the catholyte were also correspondingly higher, thus more UV light would be required by them, leading to less UV exposure for H_2O_2 and PS conversion and, ultimately, less $\bullet SO_4^-$ and •OH production (Chen et al., 2019).

3.2.5. *Impact of the water matrix*

Due to the complexity and variability of real water and wastewater matrices, the composition of the matrix can have a significant impact on the effectiveness of AOPs like BEF and UV/PS processes (Nadais et al., 2018; Xiao et al., 2016). Therefore, in addition to the WWTP secondary

effluent (Lyngby), three additional types of water matrices including tap water, WWTP influent (Lyngby) and secondary effluent from another WWTP (Herning) were chosen and their impact on the PPBEC process was investigated. As presented in Fig. 6, the removal rates of CBZ and CA in different water matrixes were in the following order: tap water > WWTPs secondary effluent (Lyngby) > WWTPs secondary effluent (Herning) > WWTPs influent (Lyngby). The results of one-way ANOVA further confirmed the significant impact of water quality on the degradation of CBZ and CA in the PPBEC process ($p < 0.05$, Table S3). Likewise, the calculated K_{app} values also conformed to the above order and were as follows: 1.641 ($R^2 = 0.97$), 1.326 ($R^2 = 0.98$), 1.212 ($R^2 = 0.96$), and 0.674 ($R^2 = 0.98$) h^{-1} for CBZ and 2.365 ($R^2 = 0.99$), 2.199 ($R^2 = 0.98$), 1.377 ($R^2 = 0.98$), and 0.876 ($R^2 = 0.98$) h^{-1} for CA, respectively. The reasons for K_{app} values fluctuation with different water matrixes can be summarized as follows. Firstly, NOM may compete with H_2O_2 and PS for UV radiation through photons absorption (Kong et al., 2016; Xiao et al., 2016). Secondly, the NOM and some inorganic ions (e.g., Cl^-, HCO_3^-, CO_3^{2-}, NO_3^- and NO_2^-) may also partially consume the generated $\bullet SO_4^-$ and •OH (Gu et al., 2019; Guo et al., 2013; Lu et al., 2018; Xiao et al., 2016). Notably, the scavenging of •OH by Cl^- at neutral pH (above 7.2) can be neglected according to Eq. (21) (Zou et al., 2020b).

$$\bullet OH + Cl^- \leftrightarrow \bullet HOCl^- \quad (21)$$

Although tap water typically contains far less NOM and inorganic ions (e.g., Cl^-) than the other tested water matrices, the removal efficiency of CBZ and CA wasn't significantly higher than that of influent and secondary effluents of WWTPs. This could be attributed to the high alkalinity of tap water (Table S1), as carbonate and bicarbonate can consume •OH and $\bullet SO_4^-$ (Lu et al., 2018). As expected, the influent from Lyngby WWTPs with a higher concentration of NOM and inorganic ions (e.g., Cl^-) led to a stronger inhibitory effect and the lowest pollutants removal rate amongst the water matrices tested.

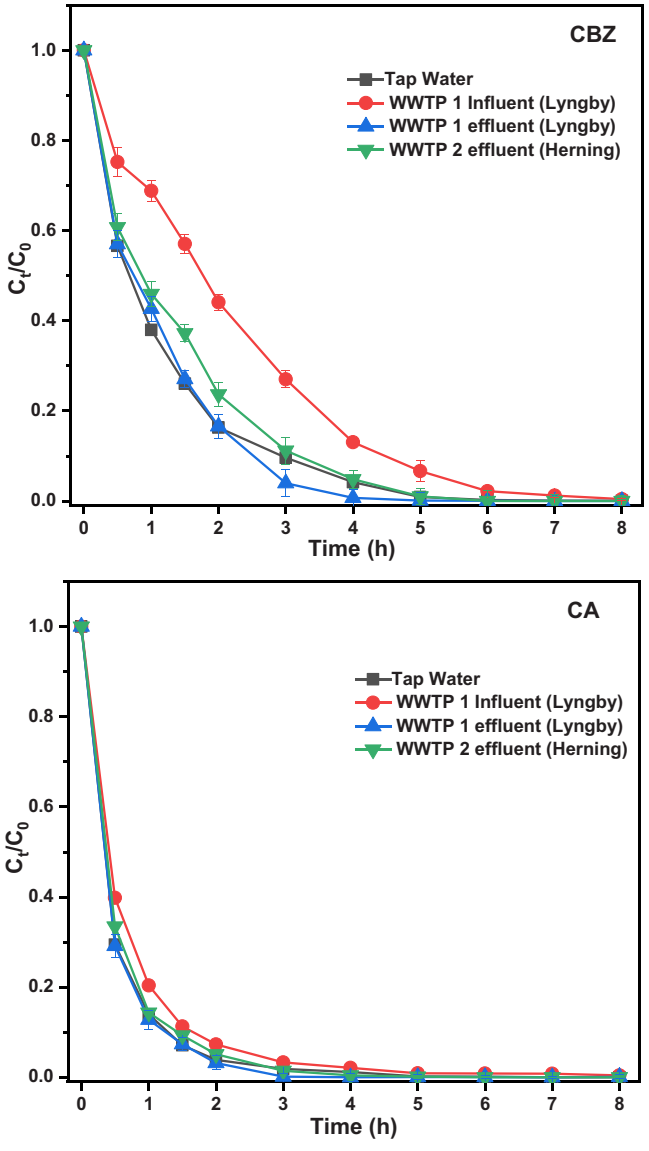

Fig. 6. The impact of water matrix on system performance. System operational parameters:.
The initial CBZ and CA concentrations of 10 mg L^{-1} were spiked into the selected water types, and other parameters were determined based on the earlier described tests, including PS dosage of 1 mM, applied voltage of 0.6 V, cathodic aeration velocity of 0.005 mL min mL^{-1}, UV intensity of 10 mW cm^{-2} and without pH adjustment.

3.3. Economic analysis

In general, the E_{EO} and corresponding Cost/O_{total} value of PPBEC process were much lower than that of UV/PS and PBEC processes (Table 1). The results indicate that the hybrid PPBEC process could reduce treatment costs by more than 93% when compared to the PBEC and UV/PS processes. Notably, the energy consumption of the UV lamp and pump for agitation accounted for 73.76% and 24.59% of the overall energy consumption, respectively. This means that both the reactor configuration and UV lamp type can be adjusted and optimized to improve the energy efficiency of UV light and further reduce energy consumption (Miklos et al., 2018). Moreover, previous reports on the UV/H_2O_2 process for wastewater treatment have verified that the scale of such treatment technology can significantly reduce energy consumption, when scaling up the process from lab-scale to pilot-scale and even further to the full-scale application (Miklos et al., 2018).

The treatment cost of the PPBEC process was further compared with some analogous technologies that have been developed for the treatment of pharmaceutical wastewaters. As shown in Table 2, ultrasound-activated PS or PMS methods consumed much more energy than the PPBEC process when treating secondary wastewater effluent (Yin et al., 2018; Zhou et al., 2016). Furthermore, individual UV, UV-activated PS, UV-activated PMS, or UV-activated H_2O_2 processes have much higher energy consumption than the PPBEC process, even at lower pharmaceutical concentrations (Deng et al., 2013; Zheng et al., 2019). In addition, the PPBEC process had both significantly lower treatment cost and higher removal efficiency than the BEF process (in both lab-scale and upscaled forms), without the need to adjust pH before and after treatment nor to deal with iron sludge issues (Nadais et al., 2018). Although the treatment cost of the PPBEC process was slightly higher than that of UV based photocatalysis using a PVDF membrane with immobilized TiO_2, it was still within the same order of magnitude

Table 1
Economic analysis for the removal of CBZ and CA in the PPBEC system.

Treatment process	UV/PS	PBEC	PPBEC
K_{app} (h^{-1})	0.310	0.343	1.385
$E_{EO/UV}$ (kWh m^{-3} $order^{-1}$)	1016.13	918.37	64.98
$E_{EO/agitation}$ (kWh m^{-3} $order^{-1}$)	338.71	306.13	21.66
$E_{EO/aeration}$ (kWh m^{-3} $order^{-1}$)	0	20.53	1.44
$E_{EO/MEC}$ (kWh m^{-3} $order^{-1}$)	0	0.12	0.02
$E_{EO/total}$ (kWh m^{-3} $order^{-1}$)	1354.84	1245.15	88.10
Cost/O_{UV} (€ m^{-3} $order^{-1}$)	254.03	229.59	16.25
Cost/$O_{agitation}$ (€ m^{-3} $order^{-1}$)	84.68	76.53	5.42
Cost/$O_{aeration}$ (€ m^{-3} $order^{-1}$)	0	5.13	0.36
Cost/O_{MEC} (€ m^{-3} $order^{-1}$)	0	0.03	0.01
Cost/O_{PS} (€ m^{-3} $order^{-1}$)	0.15	0	0.15
Cost/O_{total} (€ m^{-3} $order^{-1}$)	338.86	311.29	22.18

Table 2
Comparison of energy consumption on the removal of pharmaceuticals via different treatment technologies.

Treatment technologies	Water types	Pharmaceuticals types	Initial concentration (mg L^{-1})	Degradation efficiency	Energy consumption (E/EO, kWh m^{-3})	Treatment cost (€ m^{-3})	Reference
Ultrasound/Fe^0/PS	Deionized water	Sulfadiazine	20	90%	185.7	–	(Zhou et al., 2016)
Ultrasound/peroxymonosulfate	Drinking wtaer	Sulfamethazine	50	99% in 30 mins	1510	–	(Yin et al., 2018)
UV and UV/CaO_2	Secondary wastewater effluent	CBZ and primidone (PMD)	2 of CBZ and 5 of PMD	90%	CBZ: 550.9 and 41.4; PMD: - and 108.9	–	(Zheng et al., 2019)
UV based photocatalytic by using a PVDF membrane with immobilized TiO_2	Secondary wastewater effluent	CBZ and another 4 pharmaceuticals	0.2–0.4 in total	More than 80% in 1 h	33–58	–	(Paredes et al., 2019)
Scale-up BEF process (20 L)	Deionized water	CBZ, CA and another 4 pharmaceuticals	0.5 of each	100% in 26 h	–	74.88 (only account energy)	(Zou et al., 2020a)
Lab-scale BEF process (80 mL)	Deionized water	4 of non-Steroidal Anti-Inflammatory Drugs	0.04 of each	61–97% in 5 h	–	913.46 (only account energy)	(Nadais et al., 2018)
Microbial electro-Fenton cell using Fe-Mn catalyst	Synthetic medium	CBZ	10	90% in 24 h	–	–	(Wang et al., 2018)
Biological treatment process by using white rot funguns	Secondary wastewater effluent	CBZ	5	Stable at 60% (continuous flow)	–	–	(Zhang & Geißen, 2012)
Rotating suspension cartridge reactor immobilized with funguns	Synthetic medium	CBZ	1	21% in 72 h and 60–90% (continuous flow)	–	–	(Li et al., 2016)
PPBEC process	Secondary wastewater effluent	CBZ and CA	10 of each	Approx. 100% in 4 h	88.10	22.18	In this study

- Not reported in the paper.

(33–58 vs. 88.10 kWh m^{-3}), with the benefit of a faster removal rate (Paredes et al., 2019). Biological processes are well-known to be amongst the more cost-effective treatment methods, but are also typically far less efficient for pharmaceutical and trace chemicals removal (Monteil et al., 2019). Overall, the PPBEC process shows huge potential for the removal of residual pharmaceuticals in wastewater, not only due to its high efficiency, but also due to its cost-effective nature.

3.4. Transformation products and probable pathways

The transformation products from the degradation of CBZ and CA through the PPBEC process were investigated by using HPLC-MS/MS with the *m/z* ranged from 60 to 300 in ESI positive and negative full scan modes, respectively. The system operating parameters for these trials were adopted according to the results obtained in Section 3.2.

3.4.1. CBZ

Total ion chromatography and MS2 spectra showed that ten major transformation products were produced during the PPBEC treatment process (Figs. S8 and S9). These products were observed with elution times at 0.82 min (*m/z* 141.9, 102.1 and 98), 2.42 min (*m/z* 224), 3.78 min (*m/z* 180 and 109) and 6.06 min (*m/z* 196, 208, 226 and 85). Their probable molecular structures were inferred based on a combination of *m/z*, MS2 spectrum, along with related published literature, and the corresponding pathways are shown in Fig. 7a. Electron transfer in the central ring of the olefin bond CBZ with high boundary electron density caused by $\bullet SO_4^-$ generated a short-lived intermediate TP-A (*m/z* 239, not detected). This was then converted into transformation products with a *m/z* 208 (possible structures TP-B1 and B2) and a *m/z* 224 (possible structures TP-C1 and C2) by the attack of $\bullet SO_4^-$ and •OH and the loss of a group of $-CONH_2$ (Bo et al., 2017; Jelic et al., 2013; Wang and Wang, 2017; 2018b). Acridine-9-carboxaldehyde has been previously identified in the degradation of CBZ by AOPs (e.g. ozonation and photocatalytic processes), with a *m/z* 208 (Azaïs et al., 2017; Bo et al., 2017). Interestingly, this transformation product was not found by standard product verification within our study (Fig. S10). The transformation product of *m/z* 208 was found to be further converted into intermediates *m/z* 226 (possible structures TP-D1 and D2) and *m/z* 180 (possible structure TP-E) through •OH addition followed by ring contraction (Bo et al., 2017; Jelic et al., 2013; Wang and Wang, 2017; 2018b). The products of TP-C1, TP-C2 and TP-E were further hydroxylated to intermediate *m/z* 196, with four possible structures highlighted by literature (Azaïs et al., 2017; Bo et al., 2017; Jelic et al., 2013). Finally, $\bullet SO_4^-$ and •OH radicals caused cleavage of the benzene ring to produce various small molecular transformation products (TP-G to TP-K) which were eventually converted into CO_2 and H_2O (Bo et al., 2017; Jelic et al., 2013). Fig. S11 also shows the trend of the abundance of various transformation products of CBZ versus time. Notably, the results indicate that all transformation products first increased and but then decreased in abundance as the reaction proceeds, and were finally completely removed.

3.4.2. CA

In addition to CBZ, the degradation products of CA were also investigated to infer its possible degradation pathways. Since the structure of CA was less complex than CBZ, it was easier to remove and mineralize accordingly. Therefore, unlike the CBZ degradation process which detected many products, only a few were detected during CA degradation (Figs. S12 and S13). Specifically, three major transformation products were detected, with elution times at 3.754–4.173 min (*m/z* 168.9, 212.9 and 222.9), 5.790–6.157 min (*m/z* 168.9 and 212.9), and 6.192–6.602 min (*m/z* 168.9 and 212.9). The first transformation product corresponded to *m/z* 222.9, and the full proposed transformation pathway is presented in Fig. 7b. More specifically, CA can be transformed into *m/z* 168.9 (possible structures TP-A1 and A2) by decarboxylation, or CA was dechlorinated by substitution of •OH and then further attacked by $\bullet SO_4^-$ and •OH radicals to produce transformation product *m/z* 212.9 (possible structures TP-B) (Sun et al., 2015; Zhu et al., 2019a). Subsequently, the adjacent carbon on the benzene ring of TP-A1 was oxidized and the benzene ring was broken to produce product *m/z* 222.9 (possible structures TP-C1 and C2). A similar phenomenon has been observed in a previous study on the removal of

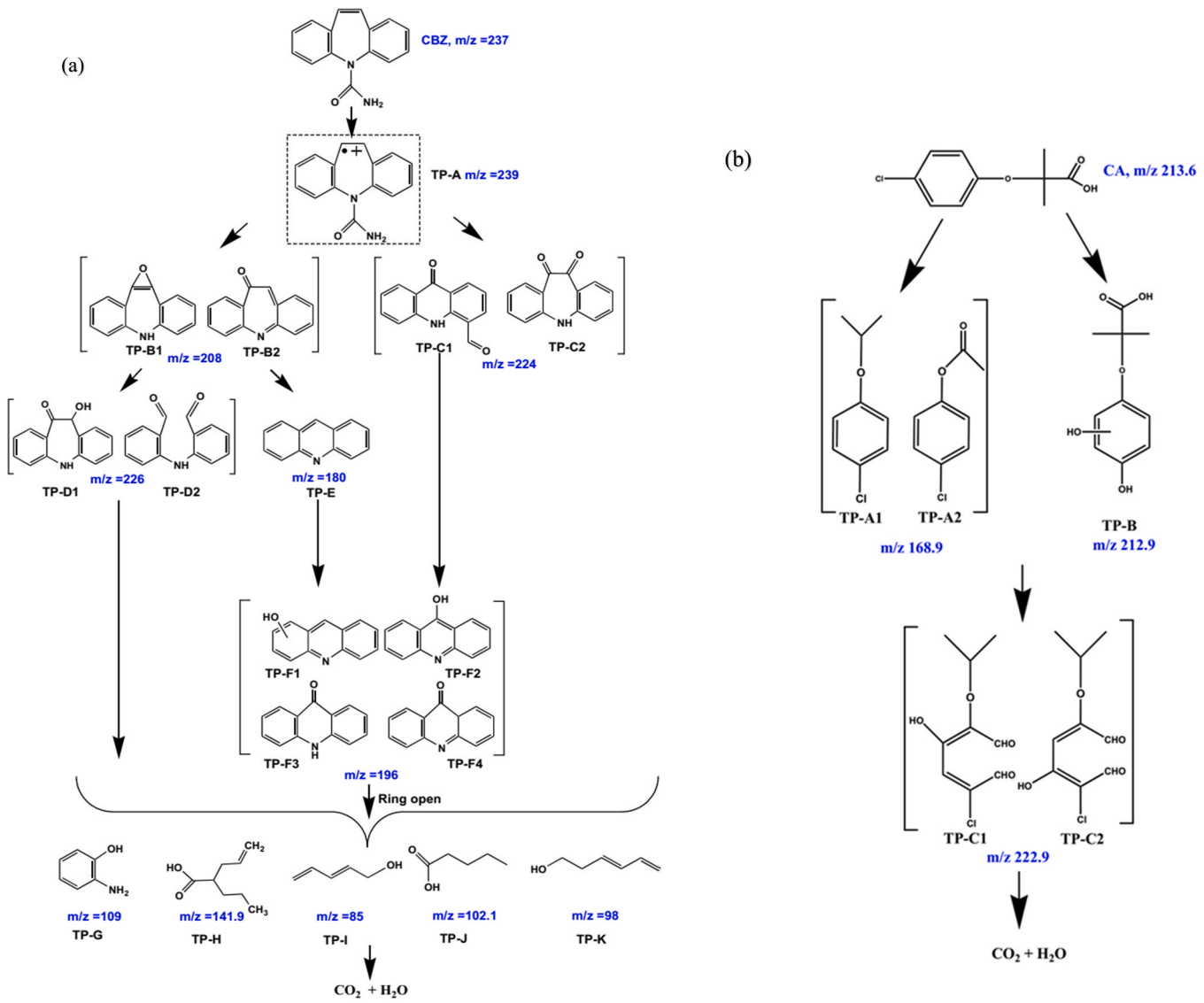

Fig. 7. Proposed transformation pathways of CBZ (a) and CA (b) in the PPBEC system.

CA by UV/O_3 and FeOOH based Fenton-like processes (Sable et al., 2015; Wang et al., 2019). Finally, TP-B,C1, and C2 were oxidized to CO_2 and H_2O. The abundance trend observed for CA degradation products was consistent to that observed for CBZ degradation (Fig. S14). This indicates that the PPBEC system has a relatively higher mineralization ability for our target pollutants than the ones that have been shown for other AOPs, such as vacuum-UV oxidation and UV/Cl_2 (Wang et al., 2016; Zhu et al., 2019b).

3.5. *Ecotoxicity assessment*

Evaluating the overall effectiveness and eco-friendliness of new proposed technology should be documented according to not only the removal efficiency of target pollutants, but also by a toxicity assessment of the degradation products. For example, some AOPs (e.g., gamma irradiation and ozonation) have been found to produce highly toxic intermediate products during the treatment of pharmaceutical-containing wastewater (Stalter et al., 2010) which can limit their applications. Therefore, the ecotoxicity assessment for samples before and after treatment through the PPBEC process was carried out. This was done by comparing the widely-used luminescence inhibition effect of *Vibrio fischeri*, with assay times of 10 and 20 min. As shown in Fig. 8, the percentage of bacterial luminescence inhibition at assay time of 10 and 20 min fluctuated around 10% throughout the whole treatment process, showing a slight increase first and then a continuous decrease and finally lower than the initial value before treatment. The ecotoxicity of compounds like CBZ was found in previous studies (Deng et al., 2017; Lai et al., 2021). Thus, this indicates that the ecotoxicity of water samples did not increase significantly during the treatment process and was eventually reduced. A similar phenomenon has been observed on CBZ degradation by the catalytic activation of PMS (Deng et al., 2017). It has been previously found that the ecotoxicity of CBZ and CA removal by direct UV photolysis, photocatalysis or ozonation process tended to be monotonically increased because some of the resulting transformation products (e.g., acridine and hydroxyl-CA) were more toxic than the parent compounds (Donner et al., 2013; Zhu et al., 2019b). It is important to note that since the ecotoxicity assessment in this work only involved *Vibrio fischer,* the specific ecotoxicity results should only be used as an indicator rather than simply extending the results to other species. Nevertheless, the results still indicate that the PPBEC process could be considered as an efficient and environment-friendly water treatment technology.

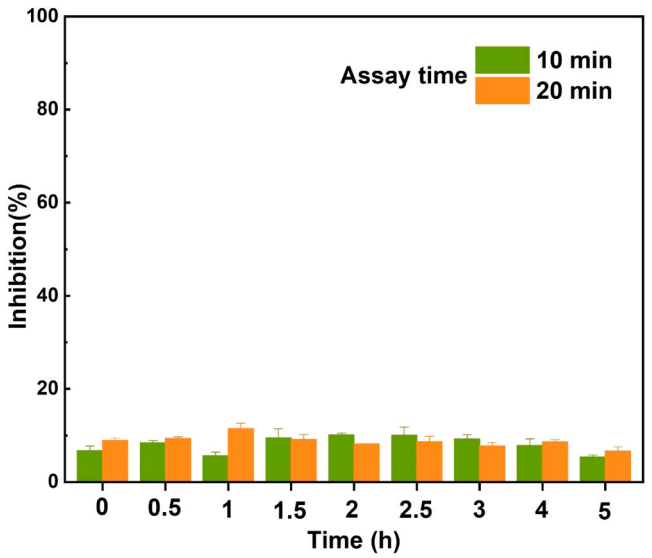

Fig. 8. Eco-toxicity assessment at two assay times (10 and 20 min) in terms of inhibition (%) of the luminescence of bacteria *Vibrio Fischeri* on the removal of CBZ and CA through the PPBEC process. Operating conditions: CBZ and CA were spiked into the WWTPs secondary effluent (Lyngby) to reach concentrations of 10 mg L^{-1}, PS dosage of 1 mM, applied voltage of 0.6 V, cathodic aeration velocity of 0.005 mL min mL^{-1}, UV intensity of 10 mW cm^{-2}, reaction time at 5 h and without pH adjustment.

3.6. Implications

This work for the first time verified the feasibility and applicability of using this novel PPBEC system to effectively to remove residual refractory micropollutants from WWTPs secondary effluent. The PPBEC system has several advantages over traditional UV based AOPs (e.g., UV/PS and UV/H_2O_2/PS) and the recently proposed BEF and MEUC systems, in terms of treatment efficiency, resilience to high chromaticity and turbidity and feasibility of treatment at neutral pH. Though promising, the following challenges should be addressed before field application. Firstly, membrane fouling could be occurred after long-term operation. Secondly, high capital cost (e.g., electrodes and membranes) for the reactor construction. Thirdly, the reactor configuration should be further improved to improve the efficiency of UV utilization together with further reducing energy consumption required by aeration. To meet the above challenges, future efforts should be devoted to the development of new membrane and electrode materials that are inexpensive and have strong anti-pollution capabilities (Asghar et al., 2015). Moreover, some of the EF reactor design (e.g., flow-through and photo EF reactor configurations) could be further developed and employed for PPBEC process (Li et al., 2018).

4. Conclusions

An innovative PPBEC system was developed and successfully operated for the efficient and cost-effective removal of model refractory micropollutants CBZ and CA. This was achieved at a low PS dosage of 1 mM, input voltage of 0.6 V, cathodic aeration velocity of 0.005 mL min mL^{-1}, UV intensity of 10 mW cm^{-2}, and at neutral pH throughout the process. Our results show good synergy between the bioelectrochemical-based PBEC system and the UV/PS process, whereby the synergy factor of the PPBEC system was calculated to be as high as 1.71 for CBZ and 0.56 for CA. Moreover, the PPBEC system was able to remove CBZ and CA in different water matrices. Furthermore, the transformation products of CBZ and CA were identified and the probable degradation pathways were identified. The low number of degradation products and their abundance further indicated that the PPBC process had a high mineralization capability. Ecotoxicity tests further indicated that the system was environmentally friendly and therefore has broad prospects for recalcitrant wastewater treatment.

CRediT authorship contribution statement

R. Z. and Y. Z: contributed to the conceptualization. **R. Z., K. T. and Y. Z:** designed the methodology and conducted the experiments. **A. H., R. C., M. X., X. Y., Y. S. and H. A:** contributed to the resources and the visualization. **Y. Z., and I. A:** for the funding acquisition. **R. Z:** wrote the original manuscript. **Y. Z, I. A., H. A. and Y. S:** commented on or edited the manuscript.

Declaration of Competing Interest

The authors declare that they have no known competing financial interests or personal relationships that could have appeared to influence the work reported in this paper.

Acknowledgments

Rusen Zou would like to acknowledge the China Scholarship Council, China for their financial support. Yifeng Zhang thanks The Carlsberg Foundation, Denmark for granting The Carlsberg Foundation Distinguished Fellowships (CF18–0084). This research was also supported partly by the Novo Nordisk Foundation, Denmark (NNF16OC0021568).

Appendix A. Supporting information

Supplementary data associated with this article can be found in the online version at doi:10.1016/j.jhazmat.2021.125905.

References

Ahmed, M.B., Zhou, J.L., Ngo, H.H., Guo, W., Thomaidis, N.S., Xu, J., 2017. Progress in the biological and chemical treatment technologies for emerging contaminant removal from wastewater: a critical review. J. Hazard. Mater. 323, 274–298.
Ali, F., Khan, J.A., Shah, N.S., Sayed, M., Khan, H.M., 2018. Carbamazepine degradation by UV and UV-assisted AOPs: kinetics, mechanism and toxicity investigations. Process Saf. Environ. Prot. 117, 307–314.
Asghar, A., Raman, A.A.A., Daud, W.M.A.W., 2015. Challenges and recommendations for using membranes in wastewater-based microbial fuel cells for in situ Fenton oxidation for textile wastewater treatment. Rev. Chem. Eng. 31 (1), 45–67.
Azaïs, A., Mendret, J., Cazals, G., Petit, E., Brosillon, S., 2017. Ozonation as a pretreatment process for nanofiltration brines: monitoring of transformation products and toxicity evaluation. J. Hazard. Mater. 338, 381–393.
Bo, L., He, K., Tan, N., Gao, B., Feng, Q., Liu, J., Wang, L., 2017. Photocatalytic oxidation of trace carbamazepine in aqueous solution by visible-light-driven Znln2S4: performance and mechanism. J. Environ. Manag. 190, 259–265.
Bu, L., Zhou, S., Shi, Z., Deng, L., Li, G., Yi, Q., Gao, N., 2016. Degradation of oxcarbazepine by UV-activated persulfate oxidation: kinetics, mechanisms, and pathways. Environ. Sci. Pollut. Res. 23 (3), 2848–2855.
Calisto, V., Domingues, M.R.M., Erny, G.L., Esteves, V.I., 2011. Direct photodegradation of carbamazepine followed by micellar electrokinetic chromatography and mass spectrometry. Water Res. 45 (3), 1095–1104.
Carlson, J.C., Stefan, M.I., Parnis, J.M., Metcalfe, C.D., 2015. Direct UV photolysis of selected pharmaceuticals, personal care products and endocrine disruptors in aqueous solution. Water Res. 84, 350–361.
Chen, T., Ma, J., Zhang, Q., Xie, Z., Zeng, Y., Li, R., Liu, H., Liu, Y., Lv, W., Liu, G., 2019. Degradation of propranolol by UV-activated persulfate oxidation: reaction kinetics, mechanisms, reactive sites, transformation pathways and Gaussian calculation. Sci. Total Environ. 690, 878–890.
Chen, J.-y, Zhao, L., Li, N., Liu, H., 2015. A microbial fuel cell with the three-dimensional electrode applied an external voltage for synthesis of hydrogen peroxide from organic matter. J. Power Sources 287, 291–296.
Deng, J., Cheng, Y.-q, Lu, Y.-a, Crittenden, J.C., Zhou, S.-q, Gao, N.-y, Li, J., 2017. Mesoporous manganese Cobaltite nanocages as effective and reusable heterogeneous peroxymonosulfate activators for Carbamazepine degradation. Chem. Eng. J. 330, 505–517.
Deng, J., Shao, Y., Gao, N., Xia, S., Tan, C., Zhou, S., Hu, X., 2013. Degradation of the antiepileptic drug carbamazepine upon different UV-based advanced oxidation processes in water. Chem. Eng. J. 222, 150–158.
Donner, E., Kosjek, T., Qualmann, S., Kusk, K.O., Heath, E., Revitt, D.M., Ledin, A., Andersen, H.R., 2013. Ecotoxicity of carbamazepine and its UV photolysis transformation products. Sci. Total Environ. 443, 870–876.

Durán, A., Monteagudo, J., San Martín, I., Amunategui, F., Patterson, D., 2017. Mineralization of aniline using hydroxyl/sulfate radical-based technology in a waterfall reactor. Chemosphere 186, 177–184.
Gao, Y.-q, Gao, N.-y, Deng, Y., Yang, Y.-q, Ma, Y., 2012. Ultraviolet (UV) light-activated persulfate oxidation of sulfamethazine in water. Chem. Eng. J. 195, 248–253.
Guo, H.-G., Gao, N.-Y., Chu, W.-H., Li, L., Zhang, Y.-J., Gu, J.-S., Gu, Y.-L., 2013. Photochemical degradation of ciprofloxacin in UV and UV/H_2O_2 process: kinetics, parameters, and products. Environ. Sci. Pollut. Res. 20 (5), 3202–3213.
Gu, D., Guo, C., Hou, S., Lv, J., Zhang, Y., Feng, Q., Zhang, Y., Xu, J., 2019. Kinetic and mechanistic investigation on the decomposition of ketamine by UV-254 nm activated persulfate. Chem. Eng. J. 370, 19–26.
Jelic, A., Michael, I., Achilleos, A., Hapeshi, E., Lambropoulou, D., Perez, S., Petrovic, M., Fatta-Kassinos, D., Barcelo, D., 2013. Transformation products and reaction pathways of carbamazepine during photocatalytic and sonophotocatalytic treatment. J. Hazard. Mater. 263, 177–186.
Khan, J.A., He, X., Shah, N.S., Khan, H.M., Hapeshi, E., Fatta-Kassinos, D., Dionysiou, D. D., 2014. Kinetic and mechanism investigation on the photochemical degradation of atrazine with activated H_2O_2, $S_2O_8^{2-}$ and HSO_5^-. Chem. Eng. J. 252, 393–403.
Khan, J.A., He, X., Shah, N.S., Sayed, M., Khan, H.M., Dionysiou, D.D., 2017. Degradation kinetics and mechanism of desethyl-atrazine and desisopropyl-atrazine in water with OH and $SO_4^{\cdot-}$ based-AOPs. Chem. Eng. J. 325, 485–494.
Kong, X., Jiang, J., Ma, J., Yang, Y., Liu, W., Liu, Y., 2016. Degradation of atrazine by UV/chlorine: efficiency, influencing factors, and products. Water Res. 90, 15–23.
Lai, L., Ji, H., Zhang, H., Liu, R., Zhou, C., Liu, W., Ao, Z., Li, N., Liu, C., Yao, G., 2021. Activation of peroxydisulfate by V-Fe concentrate ore for enhanced degradation of carbamazepine: surface ≡V(III) and ≡V(IV) as electron donors promoted the regeneration of ≡Fe(II). Appl. Catal. B 282, 119559.
Lin, C.-C., Lin, H.-Y., Hsu, L.-J., 2016. Degradation of ofloxacin using UV/H_2O_2 process in a large photoreactor. Sep. Purif. Technol. 168, 57–61.
Liu, H., Wang, C., Li, X., Xuan, X., Jiang, C., Cui, Hn, 2007. A novel electro-Fenton process for water treatment: reaction-controlled pH adjustment and performance assessment. Environ. Sci. Technol. 41 (8), 2937–2942.
Li, X., Chen, S., Angelidaki, I., Zhang, Y., 2018. Bio-electro-Fenton processes for wastewater treatment: advances and prospects. Chem. Eng. J. 354, 492–506.
Li, W., Lu, S., Qiu, Z., Lin, K., 2010. Clofibric acid degradation in UV254/H_2O_2 process: effect of temperature. J. Hazard. Mater. 176 (1–3), 1051–1057.
Luo, H., Li, C., Wu, C., Zheng, W., Dong, X., 2015. Electrochemical degradation of phenol by in situ electro-generated and electro-activated hydrogen peroxide using an improved gas diffusion cathode. Electrochim. Acta 186, 486–493.
Lu, X., Shao, Y., Gao, N., Chen, J., Deng, H., Chu, W., An, N., Peng, F., 2018. Investigation of clofibric acid removal by UV/persulfate and UV/chlorine processes: kinetics and formation of disinfection byproducts during subsequent chlor (am) ination. Chem. Eng. J. 331, 364–371.
Miklos, D.B., Remy, C., Jekel, M., Linden, K.G., Drewes, J.E., Hübner, U., 2018. Evaluation of advanced oxidation processes for water and wastewater treatment–A critical review. Water Res. 139, 118–131.
Monteil, H., Péchaud, Y., Oturan, N., Oturan, M.A., 2019. A review on efficiency and cost effectiveness of electro-and bio-electro-Fenton processes: application to the treatment of pharmaceutical pollutants in water. Chem. Eng. J. 376, 119577.
Moreira, F.C., Boaventura, R.A., Brillas, E., Vilar, V.J., 2017. Electrochemical advanced oxidation processes: a review on their application to synthetic and real wastewaters. Appl. Catal. B 202, 217–261.
Moztahida, M., Jang, J., Nawaz, M., Lim, S.-R., Lee, D.S., 2019. Effect of rGO loading on Fe_3O_4: a visible light assisted catalyst material for carbamazepine degradation. Sci. Total Environ. 667, 741–750.
Nadais, H., Li, X., Alves, N., Couras, C., Andersen, H.R., Angelidaki, I., Zhang, Y., 2018. Bio-electro-Fenton process for the degradation of non-steroidal anti-inflammatory drugs in wastewater. Chem. Eng. J. 338, 401–410.
Oturan, M.A., Sirés, I., Zhou, M., 2018. Electro-Fenton Process: New Trends and Scale-Up. Springer,, Singapore.
Pan, Y., Zhang, Y., Zhou, M., Cai, J., Tian, Y., 2019. Enhanced removal of emerging contaminants using persulfate activated by UV and pre-magnetized Fe^0. Chem. Eng. J. 361, 908–918.
Paredes, L., Murgolo, S., Dzinun, H., Othman, M.H.D., Ismail, A.F., Carballa, M., Mascolo, G., 2019. Application of immobilized TiO_2 on PVDF dual layer hollow fibre membrane to improve the photocatalytic removal of pharmaceuticals in different water matrices. Appl. Catal. B 240, 9–18.
Pazda, M., Kumirska, J., Stepnowski, P., Mulkiewicz, E., 2019. Antibiotic resistance genes identified in wastewater treatment plant systems–a review. Sci. Total Environ. 697, 134023.
Ramírez-Morales, D., Masís-Mora, M., Montiel-Mora, J.R., Cambronero-Heinrichs, J.C., Briceño-Guevara, S., Rojas-Sánchez, C.E., Méndez-Rivera, M., Arias-Mora, V., Tormo-Budowski, R., Brenes-Alfaro, L., 2020. Occurrence of pharmaceuticals, hazard assessment and ecotoxicological evaluation of wastewater treatment plants in Costa Rica. Sci. Total Environ. 746, 141200.
Rebelo, D., Correia, A., Nunes, B., 2020. Acute and chronic effects of environmental realistic concentrations of clofibric acid in Danio rerio: behaviour, oxidative stress, biotransformation and lipid peroxidation endpoints. Environ. Toxicol. Pharmacol. 80, 103468.
Sable, S.S., Ghute, P.P., Álvarez, P., Beltrán, F.J., Medina, F., Contreras, S., 2015. FeOOH and derived phases: efficient heterogeneous catalysts for clofibric acid degradation by advanced oxidation processes (AOPs). Catal. Today 240, 46–54.
Stalter, D., Magdeburg, A., Oehlmann, J., 2010. Comparative toxicity assessment of ozone and activated carbon treated sewage effluents using an in vivo test battery. Water Res. 44 (8), 2610–2620.
Sun, Q., Wang, Y., Li, L., Bing, J., Wang, Y., Yan, H., 2015. Mechanism for enhanced degradation of clofibric acid in aqueous by catalytic ozonation over MnOx/SBA-15. J. Hazard. Mater. 286, 276–284.
Thanekar, P., Panda, M., Gogate, P.R., 2018. Degradation of carbamazepine using hydrodynamic cavitation combined with advanced oxidation processes. Ultrason. Sonochem. 40, 567–576.
Wang, Y., Li, H., Yi, P., Zhang, H., 2019. Degradation of clofibric acid by UV, O3 and UV/O3 processes: performance comparison and degradation pathways. J. Hazard. Mater. 379, 120771.
Wang, J., Wang, S., 2018a. Activation of persulfate (PS) and peroxymonosulfate (PMS) and application for the degradation of emerging contaminants. Chem. Eng. J. 334, 1502–1517.
Wang, S., Wang, J., 2017. Carbamazepine degradation by gamma irradiation coupled to biological treatment. J. Hazard. Mater. 321, 639–646.
Wang, S., Wang, J., 2018b. Degradation of carbamazepine by radiation-induced activation of peroxymonosulfate. Chem. Eng. J. 336, 595–601.
Wang, W.-L., Wu, Q.-Y., Huang, N., Wang, T., Hu, H.-Y., 2016. Synergistic effect between UV and chlorine (UV/chlorine) on the degradation of carbamazepine: influence factors and radical species. Water Res. 98, 190–198.
Xiao, Y., Zhang, L., Zhang, W., Lim, K.-Y., Webster, R.D., Lim, T.-T., 2016. Comparative evaluation of iodoacids removal by UV/persulfate and UV/H_2O_2 processes. Water Res. 102, 629–639.
Xu, A., Han, W., Li, J., Sun, X., Shen, J., Wang, L., 2016. Electrogeneration of hydrogen peroxide using Ti/IrO_2–Ta_2O_5 anode in dual tubular membranes Electro-Fenton reactor for the degradation of tricyclazole without aeration. Chem. Eng. J. 295, 152–159.
Xu, Z., Shan, C., Xie, B., Liu, Y., Pan, B., 2017. Decomplexation of Cu (II)-EDTA by UV/persulfate and UV/H_2O_2: efficiency and mechanism. Appl. Catal. B 200, 439–447.
Yin, R., Guo, W., Wang, H., Du, J., Zhou, X., Wu, Q., Zheng, H., Chang, J., Ren, N., 2018. Enhanced peroxymonosulfate activation for sulfamethazine degradation by ultrasound irradiation: performances and mechanisms. Chem. Eng. J. 335, 145–153.
Yuan, F., Hu, C., Hu, X., Qu, J., Yang, M., 2009. Degradation of selected pharmaceuticals in aqueous solution with UV and UV/H_2O_2. Water Res. 43 (6), 1766–1774.
Yu, X., Gocze, Z., Cabooter, D., Dewil, R., 2021. Adsorption-photocatalysis synergistic removal of contaminants under antibiotic and Cr(VI) coexistence environment using non-metal g-C3N4 based nanomaterial obtained by supramolecular self-assembly method. J. Hazard Mater. 404, 124171.
Yu, X., Zhou, M., Ren, G., Ma, L., 2015. A novel dual gas diffusion electrodes system for efficient hydrogen peroxide generation used in electro-Fenton. Chem. Eng. J. 263, 92–100.
Zhang, Q., Chen, J., Dai, C., Zhang, Y., Zhou, X., 2015. Degradation of carbamazepine and toxicity evaluation using the UV/persulfate process in aqueous solution. J. Chem. Technol. Biotechnol. 90 (4), 701–708.
Zhang, Y., Geißen, S.-U., 2012. Elimination of carbamazepine in a non-sterile fungal bioreactor. Bioresour. Technol. 112, 221–227.
Zhao, C., Si, B., Mirza, Z.A., Liu, Y., He, X., Li, J., Wang, Z., Zheng, H., 2017. Activated carbon fiber (ACF) enhances the UV/EF system to remove nitrobenzene in water. Sep. Purif. Technol. 187, 397–406.
Zheng, M., Daniels, K.D., Park, M., Nienhauser, A.B., Clevenger, E.C., Li, Y., Snyder, S.A., 2019. Attenuation of pharmaceutically active compounds in aqueous solution by UV/CaO_2 process: influencing factors, degradation mechanism and pathways. Water Res. 164, 114922.
Zhou, L., Hu, Z., Zhang, C., Bi, Z., Jin, T., Zhou, M., 2013. Electrogeneration of hydrogen peroxide for electro-Fenton system by oxygen reduction using chemically modified graphite felt cathode. Sep. Purif. Technol. 111, 131–136.
Zhou, T., Zou, X., Mao, J., Wu, X., 2016. Decomposition of sulfadiazine in a sonochemical Fe0-catalyzed persulfate system: parameters optimizing and interferences of wastewater matrix. Appl. Catal. B 185, 31–41.
Zhu, S., Dong, B., Wu, Y., Bu, L., Zhou, S., 2019b. Degradation of carbamazepine by vacuum-UV oxidation process: kinetics modeling and energy efficiency. J. Hazard. Mater. 368, 178–185.
Zhu, K., Wang, X., Geng, M., Chen, D., Lin, H., Zhang, H., 2019a. Catalytic oxidation of clofibric acid by peroxydisulfate activated with wood-based biochar: effect of biochar pyrolysis temperature, performance and mechanism. Chem. Eng. J. 374, 1253–1263.
Zou, R., Angelidaki, I., Yang, X., Tang, K., Andersen, H.R., Zhang, Y., 2020a. Degradation of pharmaceuticals from wastewater in a 20-L continuous flow bio-electro-Fenton (BEF) system. Sci. Total Environ. 727, 138684.
Zou, R., Hasanzadeh, A., Khataee, A., Yang, X., Xu, M., Angelidaki, I., Zhang, Y., 2021. Scaling-up of microbial electrosynthesis with multiple electrodes for in situ production of hydrogen peroxide. iScience 24 (2), 102094.
Zou, R., Tang, K., Angelidaki, I., Andersen, H.R., Zhang, Y., 2020b. An innovative microbial electrochemical ultraviolet photolysis cell (MEUC) for efficient degradation of carbamazepine. Water Res. 187, 116451.